



# Maximum Drift Demands of Earthquake Damaged Reinforced Concrete Columns Based on Residual Flexure Cracks

Bayazit Bestami Aydin<sup>1,2</sup> · Baris Binici<sup>1</sup> · Saime Selin Aktas<sup>1</sup> · Max A. N. Hendriks<sup>2,3</sup> · Kagan Tuncay<sup>1</sup>

Received: 26 September 2023 / Accepted: 16 April 2024 / Published online: 2 May 2024  
© The Author(s) 2024

## Abstract

Assessment of existing reinforced concrete (RC) structures after an earthquake is a challenging task that must somehow relate qualitative and quantitative observations in the plastic hinge regions and the associated residual deformation capacity of damaged structures. Having an estimate available for the remaining drift capacity will result in more economical and informed decisions regarding demolition or strengthening options. This study aims to develop a practical methodology to estimate the maximum drift demand of an RC column based on the residual crack width. For this purpose, fiber-based frame elements are used to model the RC column considering appropriately concrete behavior in compression and tension stiffening effects. Afterwards, the accuracy and reliability of the proposed methodology are demonstrated by validating the computational approach with two cyclic experimental results from literature and new test data for a one-bay one-story RC frame conducted within the course of this study. A comprehensive parametric study is performed for RC columns with different axial loads, longitudinal and transverse reinforcement ratios, and ground motions to exhibit the stochastic behavior. The study identifies the axial load ratio as the predominant parameter. Key findings include strong correlations between maximum drift ratios and total residual crack widths, as well as maximum compressive strains, with regression analysis yielding equations for accurate drift ratio estimation. Simple predictive models are proposed to estimate the maximum deformation demands based on observed residual crack widths. Residual cracking exceeding 5 mm poses significant risk for the columns with axial load ratios above 0.4, with 90% probability of exceedance 2% drift ratio.

**Keywords** Crack width · Reinforced concrete · Column · Seismic · Drift ratio

## List of symbols

$a$	Parameter for descending of tensile curve
$a_1$	Parameter for compressive plastic offset
$a_2$	Parameter for tensile plastic offset
$f_c$	Compressive strength of concrete
$f_t$	Tensile strength of concrete

$d_b$	Diameter of the longitudinal reinforcement
$E_c$	Modulus of elasticity of concrete
$\varepsilon_{max}$	Maximum compressive strain of concrete
$\varepsilon_{cmax}$	Average maximum compressive strain of concrete
$\varepsilon_{e0}$	Elastic tensile strains at the other fiber section
$\varepsilon_{p0}$	Plastic tensile strains at the other fiber section
$\varepsilon_{cr}$	Tensile cracking strain
$\varepsilon_{c0}$	Confined strain at compressive strength
$\varepsilon_0$	Unconfined strain at compressive strength
$\varepsilon_{mc}$	Maximum compressive strain at which unloading occurs
$\varepsilon_{pc}$	Compressive plastic strain offset
$\varepsilon_{mt}$	Maximum tensile strain at which unloading occurs
$\varepsilon_{pt}$	Tensile plastic strain offset
$k_c$	Post-peak confined compressive shape factor
$k$	Post-peak unconfined compressive shape factor
$l$	Length of shear span
$l_p$	Plastic hinge length
$S_r$	Crack spacing
$N$	Axial load
$n$	Axial load ratio
$n_c$	Number of cracks
$A_g$	Gross cross sectional area
$f_{y,l}$	Yield strength of longitudinal rebar
$f_{u,l}$	Ultimate strength of longitudinal rebar
$\varepsilon_{ult}$	Ultimate strain of longitudinal rebar
$f_{y,t}$	Yield strength of transverse rebar
$p_x$	X-direction pinching factor
$p_y$	Y-direction pinching factor
$d_1$	Ductility damage parameter
$d_2$	Energy damage parameter
$\rho_l$	Longitudinal reinforcement ratio
$\rho_s$	Transverse reinforcement ratio
$T_{target}$	Target fundamental period
$R$	Reduction factor
$R^2$	Coefficient of determination
$S_r$	Crack spacing
$s$	Stirrup spacing
$SSR$	Sum of squares residuals
EQ	Earthquake
RC	Reinforced concrete
XFEM	Extended finite element method
CC	Correlation of coefficients
$w_{cr}$	Residual total crack width
$w_{max}$	Maximum crack width
$w_{res}$	Residual crack width
$w_t$	Total crack width
$w_i$	Ith crack width
$DR_{max}$	Maximum drift ratio
$DR_{cs}$	The smallest maximum drift ratio

$DR_{res}$	Residual drift ratio
$\epsilon_{res}$	Residual strain value end of the motion

## 1 Introduction

Damage state of reinforced concrete (RC) members after earthquake damage is usually estimated based on visual inspection of residual crack widths, presence of concrete crushing, or rebar buckling. Although modern seismic codes provide detailed guidelines for seismic design and performance assessment of undamaged RC structures (ASCE 41-17 2017), they merely layout strategies for assessment based on post-earthquake damage. FEMA-306 (1997) and FEMA-307 (1998) propose stiffness, strength and deformation capacity reduction factors for different damage states of masonry and reinforced concrete structural walls, respectively. On the other hand, JBDPA (1991, 2014) provides seismic capacity reduction factors for RC beams, columns, and walls according to different damage classes based on an energy approach. Visual inspection for these assessments is based on the traditional methods which are subject to the inherent biases of engineering judgment (AASHTO 2017; ACI 2008). Thus, there has been a growing interest in innovative and quantitative approaches utilizing automated-based damage detection techniques for seismic evaluation of buildings in recent years such as fractal analysis (Tao et al. 2013; Luo et al. 2017; Nagarajaiah and Yang 2017; Hu et al. 2019; Hamidia and Ganjizadeh 2022; Jamshidian and Hamidia 2023). Although these methods can effectively detect cracks on concrete surfaces, few can evaluate the impact of these cracks on the overall structural capacity (Farhidzadeh et al. 2013), with disadvantages such as demanding data requirements, interpretive complexity requiring expertise, susceptibility to data noise and artifacts, and scale dependency. In recent years, the eXtended Finite Element Method (XFEM) has emerged as a powerful tool for modeling crack propagation in concrete structures since traditional finite element methods was extended to allow for the simulation of crack initiation, growth, and interaction without the need for remeshing. This technique has been increasingly applied for analyzing crack propagation and its effects on structural behavior in various RC members (Yang and Zo 2013; Yin and Zhou 2013; Yu et al. 2016, 2018). While XFEM offers promising capabilities for studying crack propagation, its application in the context of cracking mechanism and its correlation with structural performance in damaged RC columns remains relatively unexplored.

A practical parameter that can be measured on a damaged RC column appears to be the residual cracks to make a decision on the post-seismic capacity and reparability. However, residual crack widths can exhibit significant variations depending on their positions, the cyclic history of the ground motion, column axial load levels, and reinforcement amount. If one can estimate the maximum sustained drift demand of an RC column during an earthquake by observing the residual maximum crack width after the seismic event, a better estimation of the remaining drift capacity can be made. In this way, more economical and informed decisions regarding demolition or strengthening are possible.

For relatively slender RC columns with sufficient stirrups that can eliminate shear failures, flexural cracking is the major form of concrete damage. Cracks are usually observed in regions where the moment demand exceeds the cracking moment, the largest crack widths being close to plastic hinge regions (typically occurring towards the ends of columns). Depending on the history of cyclic deformation demands from the excitation and the axial force levels, the residual crack widths usually remain open. These cracks can

be especially useful for post-earthquake assessment if the maximum drift demands can be related to the measured residual crack widths. Many experimental campaigns have been conducted to observe the cyclic response of columns and beams in literature. However, studies carefully reporting the crack widths as a function of the cyclic loading history are rather scarce. Chen et al. (2009) tested RC columns with different axial loads, transverse and longitudinal reinforcement amounts and shear span to depth ratios by applying cyclic displacement excursions. In these tests, maximum crack widths at peak drift and maximum residual crack widths in each cycle were presented. It was observed that residual cracks tend to be smaller for higher axial loads and larger longitudinal reinforcement ratios. Nakano and his colleagues (Maeda et al. 2004; Nakano et al. 2007 and Takahashi et al. 2012) conducted several RC beam and column tests under monotonic and cyclic loading to quantify visible damage such as crack widths and lengths. Their work formed the basis of the JBDPA (2014) recommendations of seismic capacity reduction factors that can be used with the Japanese Seismic Performance Index. Marder et al. (2018, 2020) tested several identical ductile RC beams with and without axial restraints under monotonic, cyclic and earthquake type random cyclic loadings. Crack widths and local rotations at different drift ratios and residual displacement in each cycle were measured. It was emphasized that residual cracks in moderately damaged plastic hinge regions are merely qualitative indicators of damage rather than precise identifiers of damage states, since the crack width data from cyclic tests are not representative of the actual damage state. Chui et al. (2019) conducted reversed cyclic tests on RC columns with two different axial loads sustaining shear, flexure and shear-flexure types of failures. Modifications to the JBDPA (1991, 2014) recommendations were proposed based on these test results. Shiradhonkar and Sinha (2018) investigated the residual ratio (ratio of the residual maximum crack width to maximum crack width at the previous maximum drift ratio) based on the data provided by Chen et al. (2009). They proposed a bilinear relationship between the residual ratio and the curvature ductility demand capped at 0.55. The effect of load history, axial load ratio or the reinforcement ratio was not considered due to the scarcity of the test data.

The experimental findings outlined above show that loading history, axial load ratio and reinforcement ratio are the critical parameters affecting the residual crack widths. Moreover, due to the complexity of the cracking phenomenon, locations of cracks with the maximum widths tend to change within the plastic hinge region (Marder 2018). Therefore, instead of maximum crack width, use of the total crack width within a gauge length can be more objective as it better relates to average deformations.

While it is claimed that the maximum crack width obtained in a cyclic loading is not necessarily the same as residual crack width in shear walls (Farhidzadeh et al. 2013) and the correlation between cracked width and loss of stiffness and strength in RC component may be weak (Madani and Dolatshahi 2020), the relation of residual crack width with maximum drift demand can be more meaningful due to the nonlinearity in RC sections rather than relying solely on crack width. In addition, in relatively slender RC columns with adequate stirrups to prevent shear failures, flexural cracking predominates as the principal form of concrete damage following earthquakes, as the combination of shear and flexural cracking in RC members introduces complexity, making it challenging to establish a direct relationship between residual crack width and either maximum drift demand or maximum crack width, particularly considering that flexural cracking alone often encompasses the majority of cases post-earthquake.

The objective of this study is to propose a practical relationship between total residual crack widths in damaged RC columns with flexural cracking dominant and the maximum sustained drift demands occurring underground motions. Fiber based frame

elements are used to model the RC column considering appropriately concrete behavior in compression and tension stiffening effects. The approach is validated with the available cyclic experimental results reporting crack widths as a function of drift demands. In order to further validate the study, a one-bay one-story RC frame was tested to measure crack widths as a function of lateral drift history for the purpose of this study. Afterwards, a comprehensive parametric study is performed for RC columns with different axial loads, longitudinal and transverse reinforcement ratios under subjected to ground motions to realistically consider the seismic demands. Simple predictive models were proposed based on the results of the parametric studies to estimate the maximum deformation demands based on observed residual crack widths.

## 2 Estimating crack width from fiber based analysis

Analytical cracking analyses of RC members were conducted in numerous past studies by considering bond-slip behavior, bond stress distribution, crack spacing along with compatibility and equilibrium between the bar and the surrounding concrete (see for example Kwak and Kim 2002; Borosnyói and Balázs 2005; Castel et al. 2012; Visintin et al. 2013; Tan et al. 2020). Despite the rigorous nature of those models and their successful application to estimate behavior under service loads, their use under arbitrary cyclic deformation demands is not practical. Fiber frame elements are widely used and commonly accepted to estimate the response of RC members (Taucer et al. 1991; Spacone et al. 1996; Mazzoni et al. 2006; Scott and Fenves 2006; Fagella et al. 2013) subjected to ground motions. The usual approach to estimate crack widths with fiber-based frame elements is to modify the constitutive behavior of concrete in tension. Upon cracking of concrete, concrete can carry further tension along the uncracked regions due to stress transfer between concrete and the reinforcement. This results in a stiffening response of the bare bar surrounded with concrete, which is called tension stiffening. Hence the total force carried by the reinforcement and the surrounding concrete after cracking can practically be represented with the superposition of the bare bar and concrete tension stiffening models. The average strains within a gauge length computed by using these constitutive models can then be converted into total crack widths by using Eq. 1:

$$w_t = \sum_{i=1}^{n_c} w_i = (\varepsilon_{eo} + \varepsilon_{po})l_p \approx \varepsilon_{po}l_p \quad (1)$$

Above,  $w_t$  is the total crack width,  $w_i$  is the individual crack opening,  $n_c$  is the number of cracks within  $l_p$ ,  $\varepsilon_{eo}$  and  $\varepsilon_{po}$  are elastic and plastic tensile strains at the outer fiber section and  $l_p$  is the gauge length assumed as the plastic hinge length at the base of an RC column (Fig. 1). For less drift demand stage and consequently early-stage crack width considerations, the total micro-crack response at the plastic hinge region is represented by using the average tensile stress–strain behavior of concrete material with calibrated tensile parameters for the outer concrete fiber section. On the other hand, if flexural cracks of columns become visible as the demands increase causing total strains well above the cracking strains, these cracks are characterized as macro-cracks and  $\varepsilon_{eo}$  becomes negligible. Furthermore, the presence of micro-cracks near macro-crack tips with softening response are also accounted for the combined nonlinearity of macro and micro-cracking mechanisms in the average tensile stress–strain response of concrete. Thus, plastic tensile strains at the outer fiber section are associated with complicated cracking mechanisms,

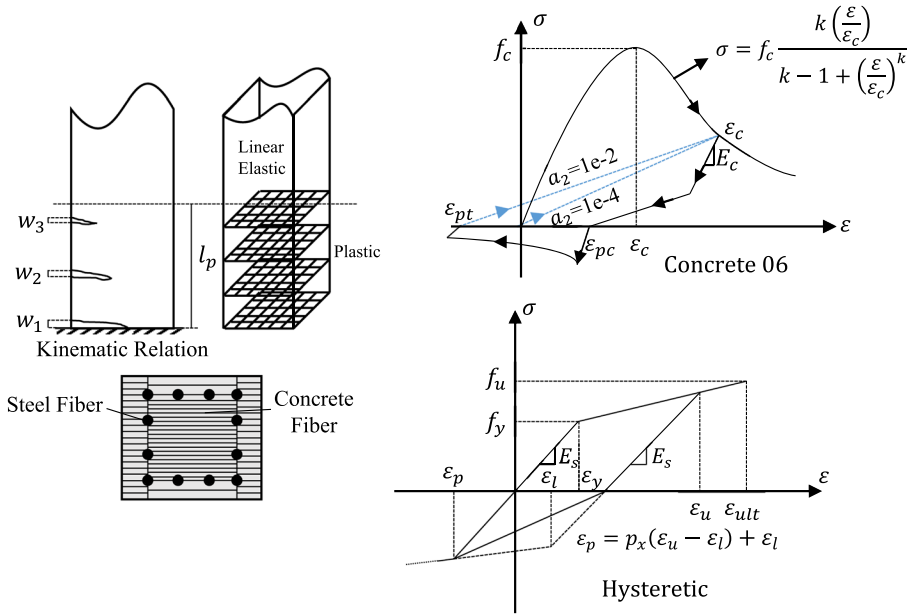


**Fig. 1** Numerical modeling with *beam with hinges* elements with fiber cross-section integration in the plastic hinge zones of length  $l_p$ , and average stress–strain relationships for concrete and steel

from the early stages of micro-crack formation to the emergence of visible macro-cracks, considering combined nonlinearity in fiber sections. For the considered gauge length, we assume the plastic hinge length based on Paulay and Priestley (1992) given with Eq. 2:

$$l_p = 0.08l + 0.022d_b f_{y,l} \tag{2}$$

where  $l$  is the length of the shear span,  $d_b$  and  $f_{y,l}$  are the diameter and yield strength of the steel longitudinal reinforcement. In this way, the total crack width occurring in the plastic hinge zone is related to the plastic strain demands, which can be estimated with fiber-based frame elements.

The simulations were conducted by using the OpenSees Platform (McKenna and Fenves 2000). The model uses *beam with hinges* elements with fiber cross-section integration in the plastic hinge zones, in which  $l_p$  is calculated with Eq. 2 or obtained from experiment. The elastic part of the element was modeled with an effective flexural rigidity in compliance with ASCE-SEI 41 (2017). Cross sectional properties of these elements were driven from fiber sections. The section was divided into confined and unconfined regions and steel layers (Fig. 1). The use of average stress–strain relationships for concrete in tension and compression is a crucial part of this approach to estimate the crack widths accurately. Appropriate constitutive models were assigned in order to represent the average stress–strain relations of RC members as shown in Fig. 1. For concrete fiber elements in compression Popovics (1973) equation was used and the parameters were selected by using the Mander Model (1988) (i.e. Concrete 06) for the confined and unconfined concrete behavior, which determines the uniaxial compression response parameters for the concrete material. The unloading in compression was calculated with the initial stiffness until the strain

at which unloading stiffness changes to 7.1% of the initial stiffness as suggested by Palermo and Vecchio (2003). The compressive plastic strain offset is computed using the following expression:

$$\epsilon_{pc} = \epsilon_{mc} \left( 1 - e^{-\alpha_1 \left( \frac{\epsilon_{mc}}{\epsilon_{c0}} \right)} \right) \tag{3}$$

Above,  $\epsilon_{mc}$  is the maximum compressive strain at which unloading occurs, and  $\alpha_1$  is a parameter controlling the plastic offset and taken as 0.32. Belarbi and Hsu (1994) model was used to model the tension stiffening behavior of concrete as given by Eq. 4:

$$\sigma_t = \begin{cases} E_c \epsilon & \text{for } \epsilon \leq \epsilon_{cr} \\ E_c \epsilon_{cr} \left( \frac{\epsilon_{cr}}{\epsilon} \right)^\alpha & \text{for } \epsilon_{cr} < \epsilon \end{cases} \tag{4}$$

where  $E_c$  is the elasticity modulus of concrete,  $\epsilon$  is the tensile strain,  $\epsilon_{cr}$  is the tensile cracking strain and  $\alpha$  is a parameter controlling the descending region of the curve, which is taken as 4 as suggested by Belarbi and Hsu (1994). The unloading branch of the tensile loading regime is assumed to be linear with a plastic strain calculated using the following equation:

$$\epsilon_{pt} = \epsilon_{mt} \left( 1 - e^{-\alpha_2 \left( \frac{\epsilon_{mt}}{\epsilon_{cr}} \right)} \right) \tag{5}$$

Above,  $\epsilon_{mt}$  is the maximum tensile strain at which unloading occurs, and  $\alpha_2$  is a parameter controlling the plastic offset. The value of plastic offset plays an important role in the estimations of residual crack widths. In this study, two extreme values of tensile plastic strain value ( $\alpha_2 = 0.01$  and  $0.0001$ ) were used to investigate the influence of the tensile plastic strain offset on the residual cracks and the overall sensitivity. The difference between these extreme values is shown in Fig. 1. For steel fiber elements, a bilinear envelope curve was used to include strain hardening with a post yield stiffness obtained by joining the yield point with the ultimate. Cyclic behavior of the reinforcing bar was modeled using the Hysteretic Material to incorporate bond-slip and pinching effects. The bilinear backbone points for steel response were derived from mechanical properties outlined in Table 1 with the modulus of elasticity value of 200 GPa. While damage effects resulting from ductility or energy were considered negligible and very small numbers were used to vanish the effects as an input, pinching plays an important role in the unloading and reloading phases of reinforcing bars for RC sections. For simplicity, only the strain direction effect was focused for this response, setting  $p_y$  to 1.0. Thus, the hysteretic model parameters shown in Fig. 1 and Table 1 with no damage and only pinching in strain direction were calibrated by matching the measured load–displacement response with the numerical result of one test (CYC specimen from Marder et al. 2018, 2020) presented in the next section. In the remaining simulations from the study of Marder et al. (2018, 2020), Chen et al. (2009), and the experiment presented in this study, all calibrated hysteresis parameters were kept constant to have objective results. Tests were simulated by applying the cyclic deformation demands while applying the axial load prescribed in the test. Second order effects were accounted for in the simulations. For all simulations in this study, the parameters to create beam elements composed of concrete and steel fibers as mentioned are listed in Table 1.

**Table 1** The properties of beams and columns

Prop	Marder et al. (2018)			Chen et al. (2009)		Experiment in this study		Parametric study		
	MONO	CYC	LER	ER	Column	Beam	$\rho_s(\%)$	$\rho_s(\%)=0.0524$	$\rho_s(\%)=0.196$	$\rho_s(\%)=0.784$
$f_c$ (MPa)	40.5	40.9	45.6	43.0	30.3	25.0	30.3			
$E_c$ (Mpa)	39,500				30,400	23,500	30,400			
$f_t$ (Mpa)	2.23	2.24	2.36	2.30	1.927	1.75	1.927			
$\epsilon_{c0}$	-0.0033	-0.0031	-0.0032	-0.0032	-0.0055	-0.0084	-0.0059	-0.0020	-0.0025	-0.0065
$k_c$	1.548	1.558	1.697	1.617	1.325	1.261	1.334	1.993	1.716 and 1.703 and 1.285 and 1.282 and 1.691 (Ø13 and Ø18 and Ø23)	
$\epsilon_0$	-0.0020									
$k$	2.052	2.074	2.365	2.194	1.993	2.136	1.993			
$I_p$ (mm)	588*				176.9 and 142.3** (Ø14 and Ø10)	180*	240.1 and 286.3 and 332.5** (Ø13 and Ø18 and Ø23)			
$f_{y,t}$ (Mpa)	300				355 and 338 (Ø14 and Ø10)	456 and 448 (Ø8 and Ø6)	420			
$f_{u,t}$ (Mpa)	444				520 and 488 (Ø14 and Ø10)	567 and 504 (Ø8 and Ø6)	421			
$\epsilon_{ult}$	0.2				0.1	0.3	0.1			
$f_{y,t}$ (Mpa)	420				423.3	504	420			
$P_x$	0.5									
$P_y$	1.0									
$d_1$	1.0e-14									
$d_2$	1.0e-14									

\*From experimental observation, \*\*Paulay and Priestley (1992)



### 3 Simulation of residual crack widths from previous column tests

Three sets of experiments were used to evaluate the success of crack width estimations measured under cyclic load reversals. Beam tests of Marder (2018, 2020), column tests of Chen et al. (2009) and a RC frame test conducted at Middle East Technical University within the scope of this study were used for this purpose. In the experiments a reversed cyclic tip displacement history was applied to the specimen, load–deflection results along with the crack widths and spacings were collected at the maximum imposed drift ratio (or displacement) and at the unloaded deformation at zero lateral force. Test specimens had different axial load levels, which served as an appropriate way to validate the accuracy of crack width predictions under different axial load conditions. The mechanical properties of concrete and rebar in these experiments are provided in Table 1. The details of the test specimens are shown in Fig. 2. The new test conducted within the course of study was a one bay, one story frame tested to observe the crack width progression as a function of imposed drift ratio.

The first validation problem to estimate crack width with the proposed procedure consisted of the beam experiments tested by Marder et al. (2018, 2020). Four specimens labeled as “MONO”, “CYC”, “ER” and “LER” were selected. The specimens were nominally identical but exposed to different loading protocols. While the first two specimens were subjected to lateral load with no axial restraint, the other two specimens were tested under increasing axial loads, increasing as a function of the applied lateral displacements. In the experiments, the presence of axial load was due to the axial restraint on the specimen. The maximum axial load ratio  $n (N/f_c A_g)$  observed at the end of the experiment was 0.025 and 0.05 for the ER and LER specimens, respectively. In the experiments crack widths were measured at the maximum target displacement (or drift ratio) in both directions and then at the point of permanent displacement at zero load reached after unloading. Moment–curvature, and total maximum and residual crack width estimations in both directions are shown in Fig. 3. It can be observed that the crack widths tended to decrease for specimens with higher axial load at the same lateral deformation. Experimental and simulated moment–curvature responses are in good agreement. Simulation results of crack widths are shown for both extreme values of  $\alpha_2$  values and the results for the intermediate  $\alpha_2$  values are shaded to observe the influence of the unloading regime in tension on the results (as introduced in Eq. 5). The total crack widths were calculated by using Eq. 1 within the plastic hinge zone. Figure 3 shows that estimated crack width progressions are in line with the measured values. A slight overprediction of the crack widths is observed for specimen LER. Note that parameter  $\alpha_2$  hardly affected the moment–curvature predictions, however it had an effect of up to 25% for crack width predictions. Furthermore, the sensitivity analysis was conducted on the concrete material input parameters  $k_c$ ,  $k$ ,  $a$ ,  $a_1$  and  $a_2$  for the CYC specimen with the case of  $a_2$  set to 0.01 in order to understand the effect of uncertainty on the crack width estimation. In this analysis, each parameter was increased by 10% of its value in Table 1 and the resulting crack widths were compared. It is interesting to note that none of input parameters affected the crack width estimation more than about 2%. This difference was obtained from  $a_2$  parameter at the second cycle in the drift ratio of 0.54%. This finding also explains the meaning of using two extreme  $a_2$  values in the simulations. Additionally, %10 increase in the  $p_x$  parameter of steel material affected the crack width estimation at a maximum amount of 6.3% while it influenced the moment–curvature response around 10% averagely.

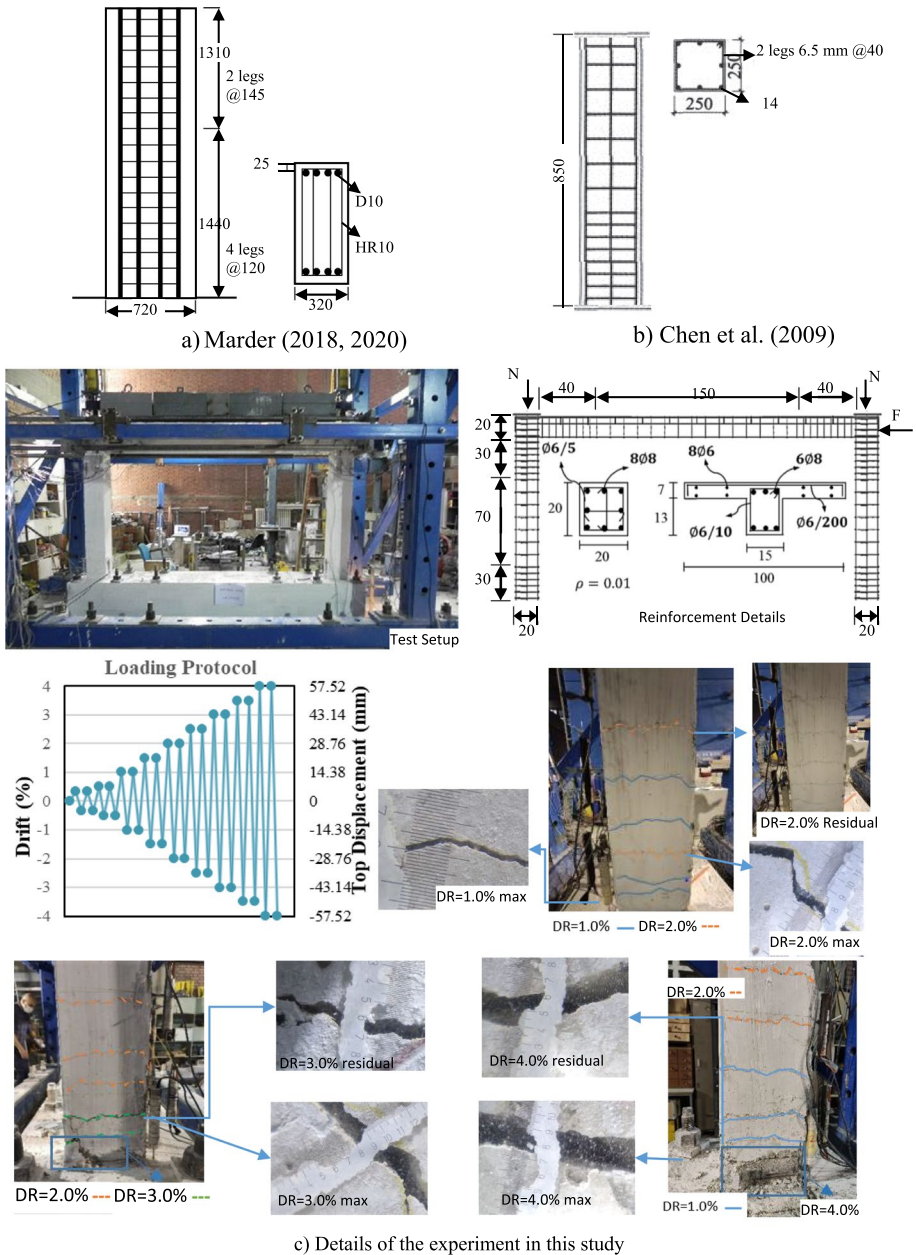


**Fig. 2** Overview of experiments used to validate crack width estimations measured under cyclic load reversals: beam tests by Marder (2018, 2020), column tests by Chen et al. (2009) and a RC frame test conducted by the authors a within the scope of this study

Chen et al. (2009) conducted horizontal cyclic loading tests of column specimens with different axial load ratios to observe the relationship between the maximum and residual crack widths as a function of drift ratios. In the study, axial load ratios (i.e. ratio of the

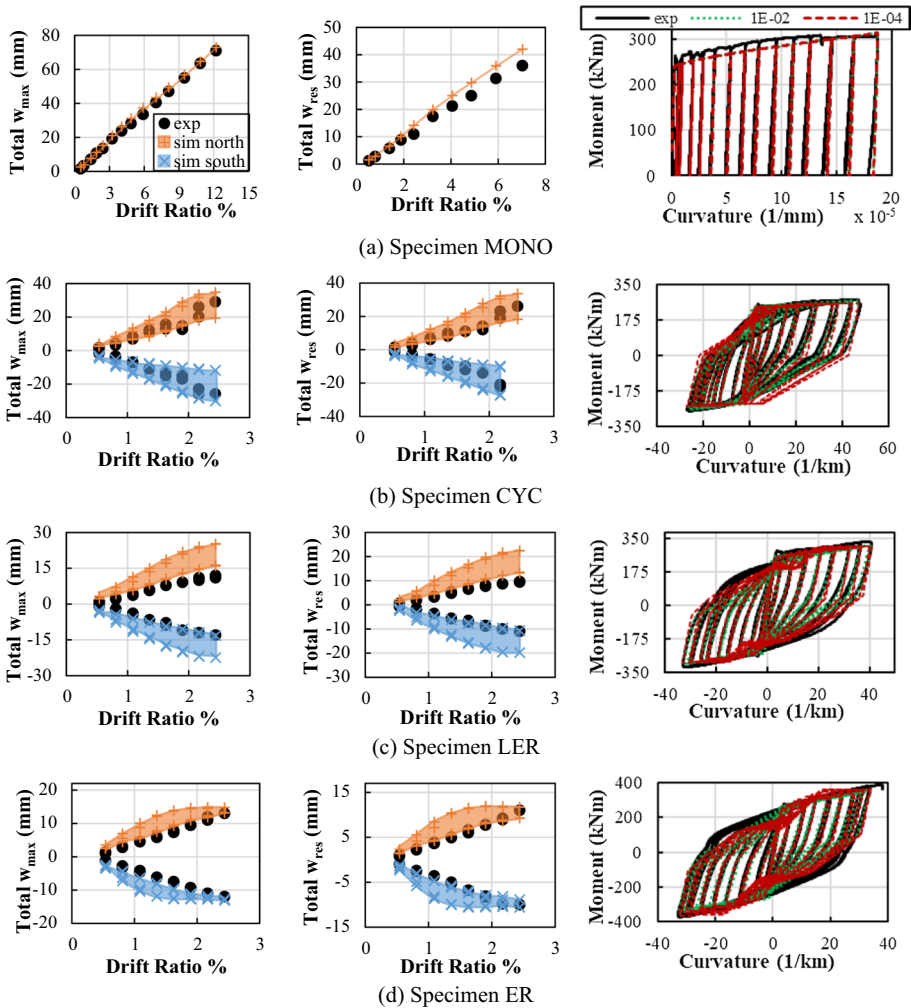


**Fig. 3** Comparisons of simulations and test results of Marder (2018, 2020) for the 4 specimens (a) MONO, (b) CYC, (c) LER and (d) ER. For each specimen respectively the total maximum crack width, the total residual crack width are given as a function of the drift ratio, in which the shaded areas indicate the effect of the  $\alpha_2$  parameter, followed by the moment–curvature relations, in which the effect of the two extreme  $\alpha_2$  values is distinguished

axial load to computed axial capacity, neglecting the steel reinforcement) were taken as 0.048, 0.144, 0.240, 0.240 and 0.336 for specimens, 301, 303, 305, 305L and 307, respectively. The lateral load tip displacement curves were reported for only two specimens (301 and 307), hence load–deflection comparisons are presented in Fig. 4 only for these specimens. Load deflection responses closely follow the experimental cyclic responses as shown in Fig. 4. Crack width results were presented for all four specimens. The estimated maximum and residual crack width values with respect to the maximum drift ratio are also presented in Fig. 4. In the experimental study, only maximum crack widths were reported, and total crack widths were not presented. In order to estimate the maximum crack widths, the

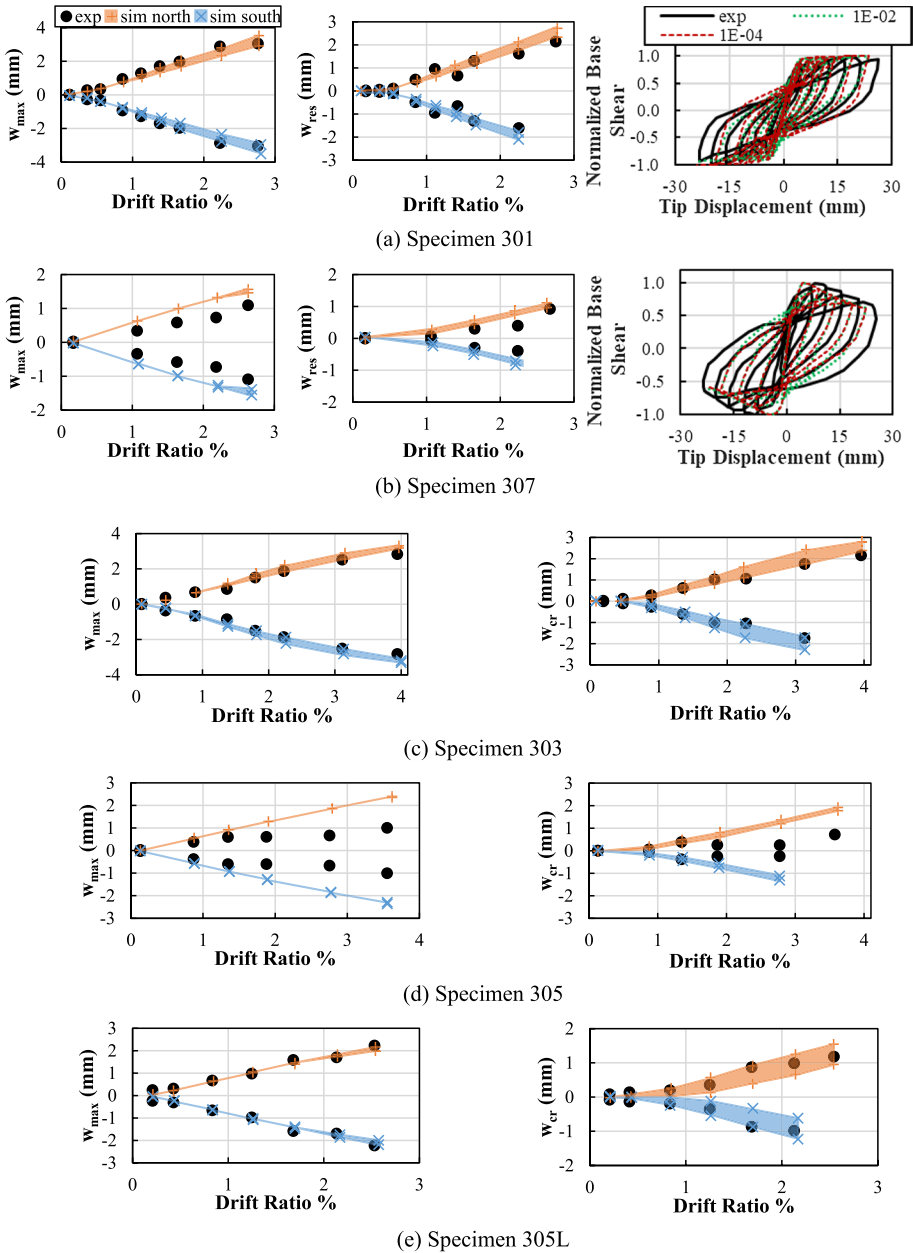


**Fig. 4** Comparisons of simulations and test results of Chen et al. (2009) for 5 specimens (a) 301, (b) 307, (c) 303, (d) 305 and (e) 305L. The maximum and residual crack width for each specimen are given as a function of drift ratio with shaded areas indicating the effect of the  $\alpha_2$  parameter. For 301 and 307 specimens, base shear and tip displacement of columns curves, distinguished the effect of two extreme  $\alpha_2$  values, are provided

average crack width in the simulations was calculated from the total crack width obtained from the simulations by dividing the total crack width with the estimated number of cracks in the plastic hinge region. The number of cracks in the plastic hinge region was estimated from  $1+S_r/l_p$  where crack spacing  $S_r$  is found from Eurocode 2. The increasing trends of the maximum and residual crack widths measured in the tests are in sufficiently good agreement with the simulation results. It is also observed that crack widths in specimen 305 are slightly overestimated. The reason can be attributed to the accuracy of crack spacing estimations. In addition, the slope of the crack width and drift ratio curve decreased significantly at the drift ratio value of about 1.4 in the experiment for specimen 305 compared to the other specimens. Note that the maximum and residual crack width estimations for the specimen 305L, having the same maximum axial load ratio  $n$  as specimen 305, closely follow the experimental results.

#### 4 Simulation of residual crack widths of the new frame test and general observations

A single-bay single-story half-scale portal frame was tested in this study for the final validation case of the proposed approach. The prepared RC frame specimen details are shown in Fig. 2. Mechanical properties of used concrete and steel rebars are listed in Table 1. The concrete compressive strength and yield strength of the steel reinforcement were 25 MPa and 420 MPa, respectively. Distributed vertical load on the slabs (10.25 kN/m) and concentrated axial forces on the columns ( $0.18 f_c A_g$ ) were applied to represent the dead load. Thus, the axial load is concentrated on the columns with an axial load ratio of 0.192. After the dead load was applied to the specimen, the lateral load was imposed with displacement control feedback to positive and negative target drift ratios. For every target drift ratio, two cycles at each identical drift ratio were applied to the test specimen. The applied lateral loading scheme is given in Fig. 2. The crack widths were measured at the positive and negative drift ratios as the maximum crack width and the load-released region as the maximum residual crack width. Magnifier lenses were used for measuring each crack at different deformation levels.

The frame failed in a flexural mode, i.e., plastic hinging of the column base and beam ends. Initial cracking was observed around 0.35%, which was followed by yielding at around 1% and cover spalling while displacing from 2 to 3% drift ratio. At the end of the test rebar buckling was observed resulting in a reduction of the lateral load carrying capacity. It can be observed that the maximum crack width increased from 0.5 mm at 2% drift ratio to 2 mm at 4% drift ratio. The ratios of the residual crack width to the maximum crack width (residual crack width ratio) were about 0.5 and 0.75 for 2% and 4% drift ratios. This shows that the residual crack width ratio tends to increase with increasing maximum deformation demands.

The simulation of the test frame was conducted using the same strategy outlined above. The results are shown in Fig. 5 for the load-deformation comparisons and crack width estimations. The capacity in the simulation was estimated to be slightly lower than the experimental results. Otherwise, the load deflection response was in good agreement with the test results. Also, the crack width estimations for both columns are shown in Fig. 5. Crack width values measured from the experiments are estimated with the proposed approach at sufficient accuracy.

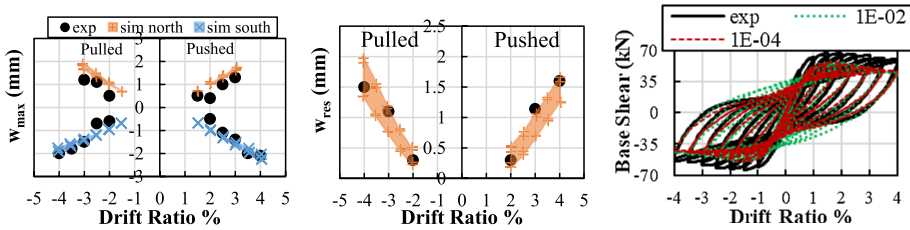


**Fig. 5** Comparisons of simulations and test results of portal frame (METU Experiment). Maximum and residual crack width for columns as a function of the drift ratio with shaded area of the impact of the  $\alpha_2$  parameter and base shear—drift ratio curve with the effect of  $\alpha_2$  parameter are shown

Based on the results of all simulations, it can be concluded that a higher tensile plastic strain value provides both higher maximum and residual crack widths. The crack width results obtained from the proposed approach were sufficiently accurate, i.e. within structural engineering accuracy, based on these validation problems. These results provide confidence in the ability of calculating crack widths in the plastic hinge zone from the average strains. As stated by Marder et. al. (2020), these results may not be representative for actual ground motion cases, which is further investigated in the next section.

### 5 Parametric study

Demands in the form of increasing displacements cannot reflect realistically the earthquake induced demands especially for residual cracks. The reversed cycles may not be imposed equally in different regions as they are more randomly distributed in the actual motions. Furthermore, the residual drift ratio and crack widths depend on the history imposed by the earthquake motion on a structure. Consequently, using actual earthquake ground motions is more reasonable to determine the relationship between the residual crack width and the maximum drift ratio. In the light of this information, a parametric study was conducted on cantilever reinforced concrete columns sustaining various levels of maximum drift demands from the applied ground motions. All columns were subjected to 11 ground motion records and they were scaled to produce different maximum drift ratios as explained below. The properties of chosen earthquake (EQ) records and acceleration spectrums are shown in Table 2 and Fig. 6 shows the unscaled response spectra of the selected motions. The column was modelled in the same way as the cantilever column test simulations, and a mass was defined at the tip of the column. Column section dimensions (400 mm × 400 mm) and reinforcement details are shown in Fig. 7. Two different reinforcement patterns that can be called code compliant and non-compliant in terms of the confining steel were used. The column length is 1.5 m representing half of a building column. The longitudinal reinforcement ratio was selected as 1.0%, 1.9%, and 3.1%, while the transverse reinforcement volumetric ratio was selected as 0.0524%, 0.1960%, and 0.7840%.

The flowchart of the performed parametric study with different parameters is shown in Fig. 7. The steps of analyses can be outlined as follows:

1. Select column  $\rho_l, \rho_s$  and define the reinforcing bar diameters to match these values
2. Select an axial load ratio  $n$  from 0.1 to 0.6 with 0.1 increments (6 values)
3. Assign a target fundamental period  $T_{target}$  0.5 to 2 s with 0.25 s. increments (7 value)

**Table 2** The properties of earthquake motions

RSN No	Earthquake	Station	Year	$M_w$	Arias intensity (m/sec)	$V_{s30}$ (m/s)	PGA (g)
779	Loma Prieta	LGPC	1989	6.9	7.9	594.8	0.57
803	Loma Prieta	WVC			1.3	347.9	0.26
1044	Northridge	NWH	1994	6.7	5.7	269.1	0.58
1063	Northridge	RRS			7.5	282.3	0.87
1084	Northridge	SCS			6.0	251.2	0.62
1086	Northridge	SYL			5.0	440.5	0.60
1503	Chi-Chi	TCU065	1999	7.6	7.7	305.9	0.79
1605	Duzce	Duzce	1999	7.1	2.9	281.9	0.40
1633	Manjil	Abbar	1990	7.4	7.5	724.0	0.51
4040	Bam	Bam	2003	6.6	8.0	487.4	0.81
8119	Christchurch	PRPC	2011	6.2	2.3	206.0	0.60

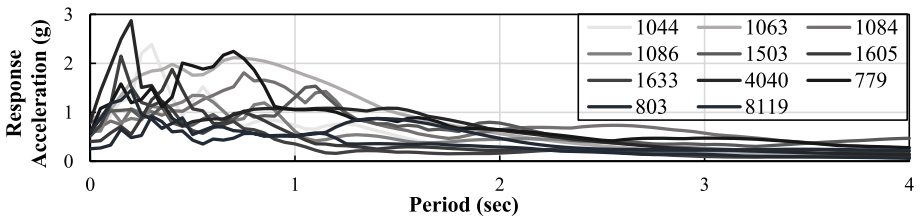


**Fig. 6** Spectra of ground motions

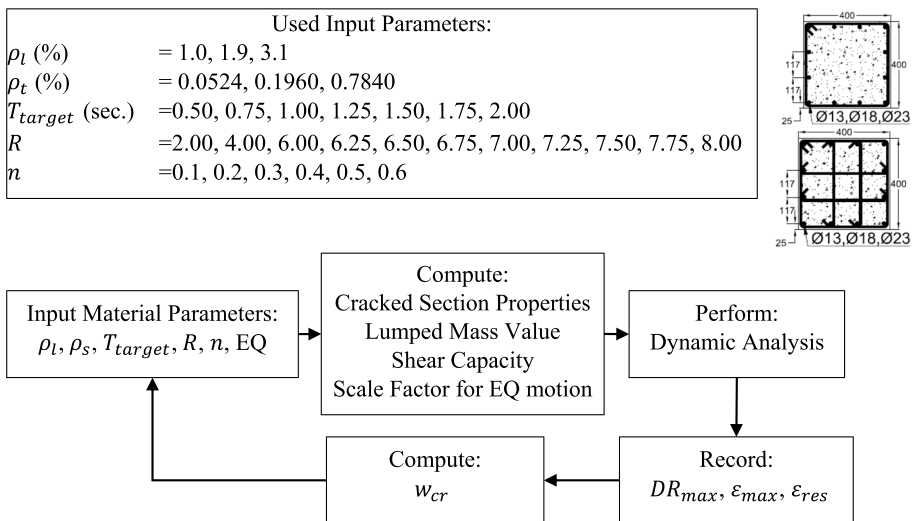


**Fig. 7** Input parameters and flowchart for dynamic analyses

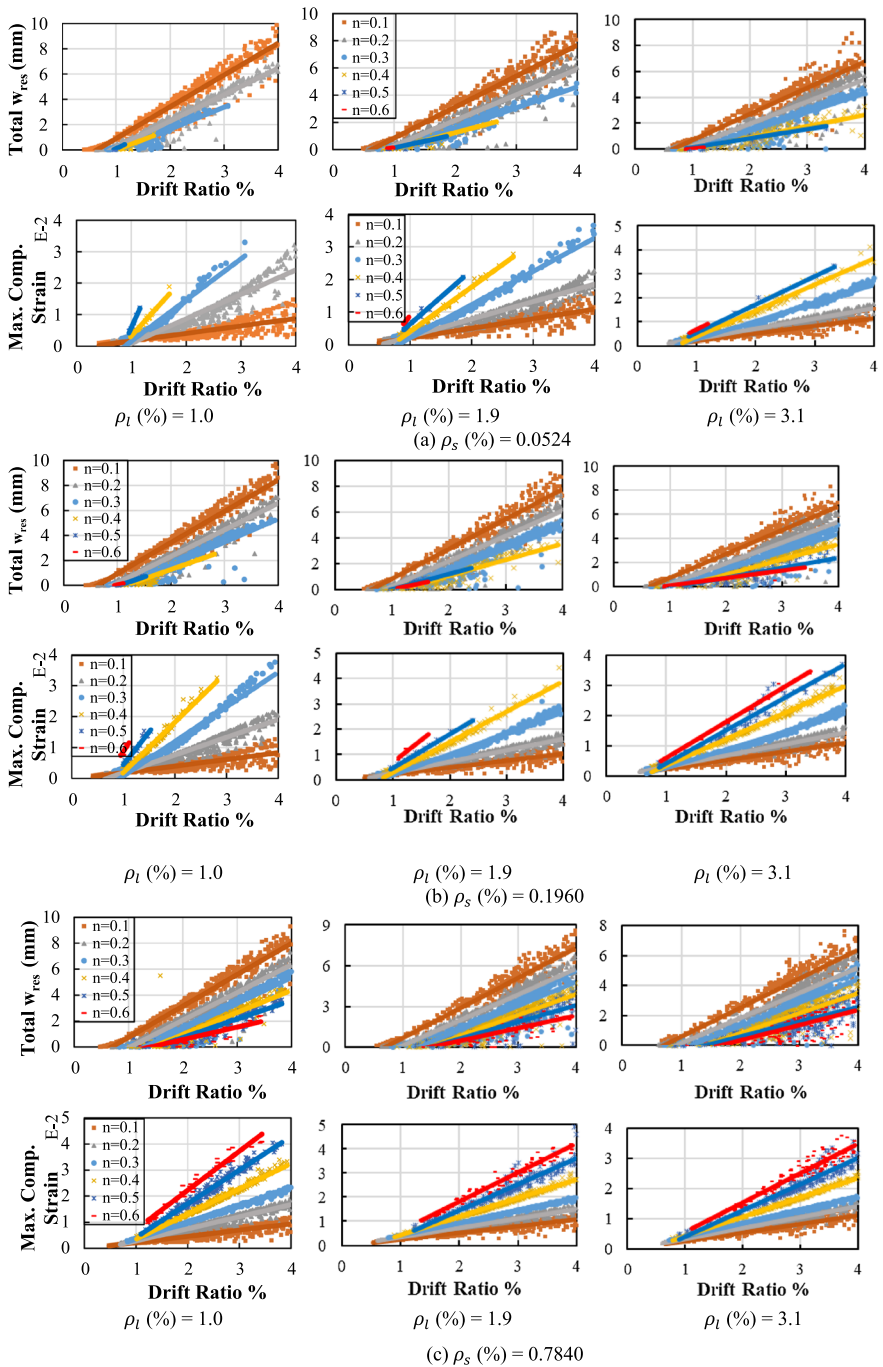
4. Compute the mass to match the  $T_{target}$  assuming cracked section rigidity according to ASCE-SEI 41-17
5. Compute the base shear capacity from the moment capacity of the column
6. Select a response modification factor  $R$  from 2 to 8 (11 values)
7. Scale the ground motion such that the ratio of the elastic base shear force (computed from the response spectral acceleration at the  $T_{target}$ ) to the base shear capacity is equal to  $R$
8. Perform the nonlinear time history analysis for each ground motion
9. Obtain the maximum drift ratio  $DR_{max}$ , residual drift ratio  $DR_{res}$ , total  $w_{max}$  and total residual crack widths  $w_{cr}$  from Eq. 1 and the maximum concrete compressive strain  $\epsilon_{max}$
10. Repeat the analysis for all sections, axial load ratios  $n$ , ground motions,  $T_{target}$ , and  $R$  factors.

Figure 8 shows the maximum drift ratio obtained during earthquake motion and the residual crack width and  $\epsilon_{max}$  results for three different longitudinal ( $\rho_l$ ) and three different transverse reinforcement ( $\rho_s$ ) ratios for the six different axial load ratios ( $n$ ). Analysis results were excluded if the maximum drift ratio was higher than 4% or divergence of the analysis indicated a collapse of the column. By employing this criterion, compression failure and subsequent stirrup rupture and rebar buckling were also implicitly taken into account as the maximum compressive strain value mostly did not exceed 0.04. A linear regression line was fitted for different axial load ratios in the plots. In Table 3, correlation of coefficients (CC) for the data corresponding to different reinforcement and axial load ratios are listed to quantify the strength and direction of the relationship between drift ratio versus total residual crack width and maximum compressive strain. Although the smallest CC value is obtained for  $n$  value of 0.6 in the correlation between drift ratio and total residual crack width which can be attributed to the relatively fewer data points than the other  $n$  values, strong positive correlations are observed with the CC values consistently close to 1 and mostly exceeding 0.80 for the relation of drift ratio with maximum compressive strain and total residual crack width. While the residual crack width increases with the increasing drift ratio demand, the increasing axial load ratio causes smaller residual cracks at the same drift ratio. The maximum compressive strain in the outer fiber of the concrete increased with increasing axial load. Although  $\rho_l$  and  $\rho_s$  are not significantly influential parameters for the residual crack widths, it can be concluded that increasing reinforcement ratio values tended to decrease permanent crack widths.

Considering the parametric study results, the most significant parameters affecting the residual crack widths are the maximum drift ratio demand and the axial load values. If the variations due to longitudinal and transverse reinforcement ratios are neglected, one can plot all the results as a function of the axial load ratio as shown in Fig. 9. Highly correlated response can still be obtained for the case of all  $p$  data gathered for different  $n$  values, as indicated by the range of CC values obtained in Table 3 from 0.800 to 0.937. It can be seen clearly that a column under high axial loads will sustain smaller residual crack widths compared to a column with smaller axial load undergoing similar maximum drift ratios. This result shows that residual cracks should always be evaluated along with the column axial loads.

The residual total crack width is a practical parameter that can be measured on-site to determine the maximum drift demand sustained by a member. If the maximum drift





**Fig. 8** Total residual crack width, maximum compressive strain at maximum drift ratio estimations for three transverse reinforcement volumetric ratios (a)  $\rho_s$  (%) = 0.0524, (b)  $\rho_s$  (%) = 0.1960 and (c)  $\rho_s$  (%) = 0.7840 and three different longitudinal reinforcement ratios,  $\rho_l$  (%) = 1.0, 1.9 and 3.1

**Table 3** The correlation coefficients of parametric studies

$\rho_f(\%)$	$\rho_s(\%)$	Total $w_{res}$ versus Drift ratio (%)					
		$n$					
		0.1	0.2	0.3	0.4	0.5	0.6
1.0	0.0524	0.9643	0.9636	0.9013	0.8783	0.9851	1.0000
	0.1960	0.9700	0.9703	0.9401	0.9083	0.9219	0.8413
	0.7840	0.9598	0.9553	0.9552	0.9302	0.9284	0.8656
1.9	0.0524	0.9598	0.9444	0.9556	0.9195	0.9183	0.5149
	0.1960	0.9607	0.9493	0.9404	0.9200	0.9388	0.9873
	0.7840	0.9565	0.9287	0.8983	0.9021	0.8423	0.8218
3.1	0.0524	0.9298	0.9183	0.9391	0.8803	0.9552	0.6635
	0.1960	0.9315	0.9103	0.9005	0.9255	0.8125	0.8827
	0.7840	0.9298	0.9047	0.9091	0.8627	0.7465	0.7430
All $\rho$ data		0.9370	0.9299	0.9224	0.9012	0.8385	0.7969
		$\epsilon_{max}$ vs Drift Ratio (%)					
1.0	0.0524	0.8013	0.9464	0.9707	0.9775	0.9824	1.0000
	0.1960	0.8299	0.9581	0.9836	0.9849	0.9696	0.8714
	0.7840	0.8921	0.9695	0.9973	0.9934	0.9819	0.9830
1.9	0.0524	0.8765	0.9627	0.9859	0.9890	0.9891	0.9598
	0.1960	0.8948	0.9594	0.9843	0.9905	0.9919	0.9771
	0.7840	0.9207	0.9657	0.9973	0.9947	0.9577	0.9773
3.1	0.0524	0.9056	0.9725	0.9894	0.9860	0.9978	0.9923
	0.1960	0.9147	0.9676	0.9873	0.9894	0.9768	0.9949
	0.7840	0.9364	0.9722	0.9960	0.9963	0.9581	0.9449
All $\rho$ data		0.8667	0.9181	0.9002	0.9258	0.9174	0.8925

ratio is known after an earthquake, one can decide on its remaining deformation capacity. By using the analyses results it is possible to propose a simple equation to estimate the maximum drift ratio ( $DR_{max}$ ) as a function of the residual total crack width ( $w_{cr}$ ) and axial load ratio ( $n$ ) with an upper limit of 0.6:

$$DR_{max} = (0.82n + 0.30)w_{cr} + (1.69n + 0.73) \tag{6}$$

This equation can be used after measuring the total residual crack width within the plastic hinge zone and estimating the axial load ratio from a simple tributary load analysis.

Similarly, one can estimate the maximum drift ratio, if the axial load ratio and average maximum compressive strain ( $\epsilon_{cmax}$ ) demand within the plastic hinge zone are known, by using:

$$DR_{max} = (-2254.6n^3 + 3411.6n^2 - 1799.3n + 422.2)\epsilon_{cmax} + (-1.4n^2 + 0.6n + 0.7) \tag{7}$$

Estimating the maximum compressive strain demand from visual post-earthquake’s observations is not possible. However, one can estimate the drift ratio demand corresponding to cover spalling by setting  $\epsilon_{cmax}$  to 0.004 (Eq. 8). In this way it is possible to know the smallest possible maximum drift ratio demand ( $DR_{cs}$ ) that the column would have displaced if cover spalling is observed after a post-earthquake.

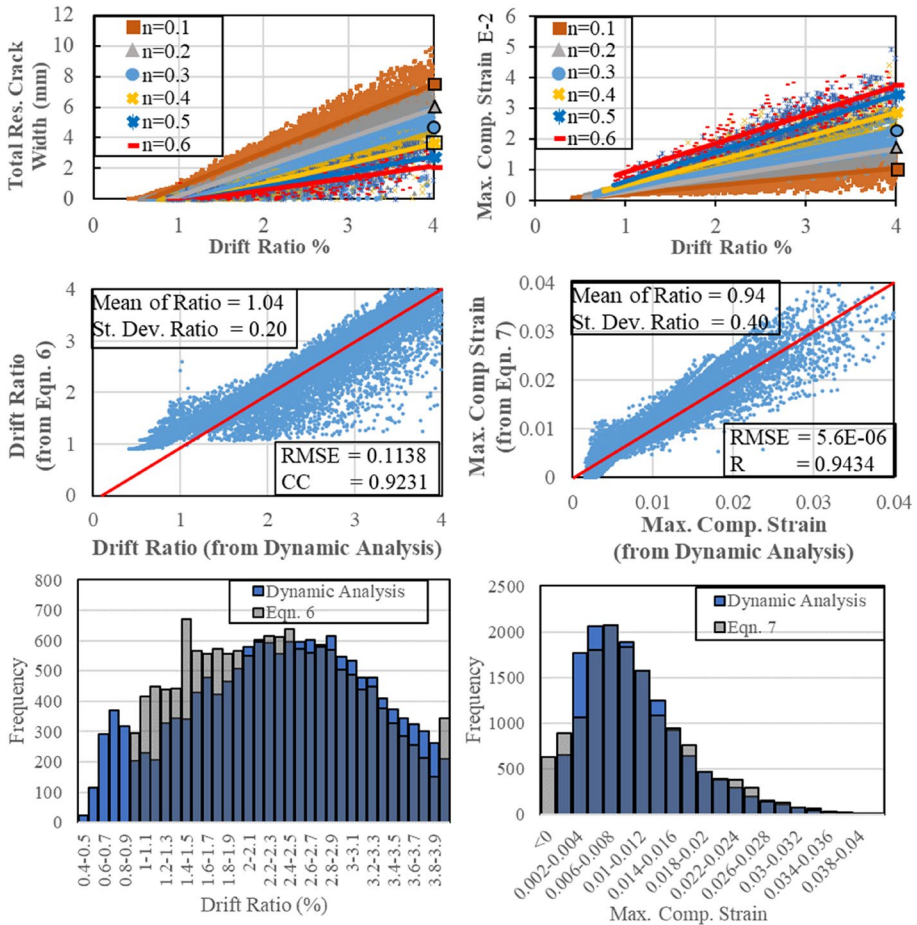


**Fig. 9** Total residual crack width, maximum compressive strain at maximum drift ratio estimations for all results and comparison with analytical and dynamic analysis results and their histograms

$$DR_{cs} = -9.02n^3 + 12.25n^2 - 6.60n + 2.39 \tag{8}$$

$DR_{max}$  and  $\epsilon_{max}$  results obtained from the Eqs. 6 and 7, and dynamic analysis results are compared in the Fig. 9 in order to exhibit the accuracy of the proposed equations. Additionally, statistical measures were employed to gauge the agreement between proposed equations and the results obtained from the dynamic analysis, achieved by calculating their respective ratios. The mean and standard deviation associated with this ratio for estimated drift ratio values deduced from the outcomes of Eq. 6 are 1.04 and 0.20, respectively. Similarly, corresponding values for the maximum compressive strain value with Eq. 7 are 0.94 and 0.40. Strong relation of obtained values from dynamic analysis and predicted values from equations for drift ratio and maximum compressive strain parameters is evident with significantly lower Root Mean Square Error (RMSE) values of 0.1138 and 5.6e-06 and higher CC values of 0.92 and 0.94 for Eqs 6 and 7, respectively. Additionally, histograms comparing these two sets of data are provided for

both quantities drift ratio and maximum compressive strain. The values from equations are consistent with the results from dynamic analysis. Thus, despite scattering, the proposed equations can estimate the maximum drift ratio that occurred during the excitations, as a function of the axial load and damage (i.e. residual crack width and possible crushing) reasonably well.

An additional validation of the proposed equation was conducted with the two column tests conducted by Marder et al. (2018). Two specimens, named LD2-LER and LD2-ER, had the same dimensions and same axial restrained conditions with the specimens of LER and ER, as mentioned above. The axial load ratios were 0.013 and 0.027 for LD2-LER and LD2-ER specimens, respectively. In the experiment, dynamic long-duration displacement history was performed for these specimens as shown in Fig. 2a. The maximum drift ratio during the loading was 2.17% for both specimens. The estimated value of the maximum drift ratio computed using Eq. 1, with the given axial load ratio and residual crack widths of 5.2 mm and 4.1 mm were 2.36% and 2.09% for LD2-LER and LD2-ER, respectively. This result provides further confidence on the accuracy of the proposed equation.

The results presented above exhibit scatter due to ground motion variability. Hence it may be convenient to plot the probability of exceeding a certain maximum drift ratio for a given crack width as shown in Fig. 10. To achieve this, the probability of exceedance for specific crack width values were calculated at various axial load ratios. For each axial load ratio, the probability of exceedance of a specified crack width value was determined by calculating the percentage of samples in which the crack widths exceed the specified value, relative to the total dataset obtained from dynamic analysis for that axial load ratio. With this way, data was prepared for 0.5%, 1%, 2% and 3% drift ratios

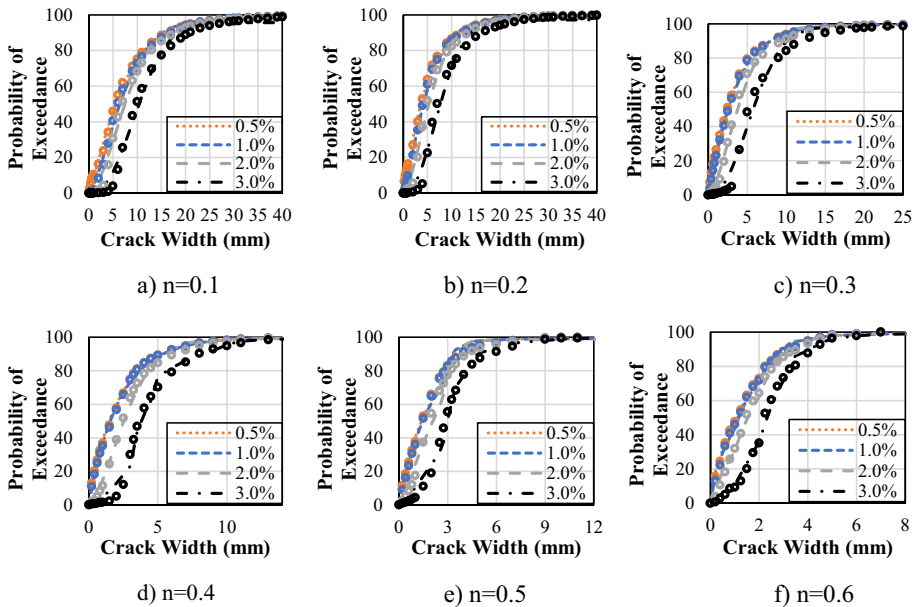


**Fig. 10** Probability curves of exceeding (four) different drift ratio values based on observed residual crack widths for 6 different axial load ratios (a)  $n=0.1$ , (b)  $n=0.2$ , (c)  $n=0.3$ , (d)  $n=0.4$ , (e)  $n=0.5$ , (f)  $n=0.6$

for 6 different axial load levels. For each of them, the curves were generated to represent the data with following generic equation:

$$Probability\ of\ exceedance = A(1 - exp(-kw_{cr}^m)) \tag{9}$$

where  $A$ ,  $k$ , and  $m$  are the constants fitted to the data by acquiring the minimum sum of the squared residuals ( $SSR$ ) between the predictive values from Eq. 9 and observed data. All values of these parameters and coefficient of determination ( $R^2$ ) are listed in Table 4. The lowest and average  $R^2$  value of 0.993 and 0.997 indicates the reliability of the formulation with the provided constants. It can be observed that smaller drift ratios would be observed with a greater probability for a given crack width. Furthermore, the increase in the axial load ratio would result in higher probability of a selected maximum drift ratio. These plots can help in making decisions about the level of inter story drift demands that a building could have sustained based on the observed residual crack widths and axial load ratios.

Finally, at the same drift ratio, the effect of the axial load ratio is presented in Fig. 11. Although results for the axial load ratio values of 0.1 and 0.2 are close to each other, at the same crack width values, a higher axial load ratio results in a higher probability for exceedance of the drift ratios of 2% and 3%. In other words, the residual crack width is being decreased by increasing the axial load ratio, as expected. It can be concluded that the same

**Table 4** The parameters for Eq. 9

$n$	Drift ratio %	$A$	$k$	$m$	$R^2$ from 0.0 to 40.0 mm crack width
0.1	0.5	98.796	0.091	1.192	0.998
	1.0	97.576	0.046	1.474	0.997
	2.0	96.912	0.021	1.753	0.995
	3.0	95.716	0.003	2.387	0.995
0.2	0.5	99.344	0.180	1.056	0.998
	1.0	98.545	0.116	1.270	0.999
	2.0	97.805	0.049	1.616	0.995
	3.0	97.047	0.009	2.178	0.993
0.3	0.5	99.623	0.310	0.977	0.999
	1.0	99.369	0.263	1.068	0.999
	2.0	98.469	0.092	1.565	0.996
	3.0	97.982	0.018	2.114	0.993
0.4	0.5	99.962	0.488	0.928	0.999
	1.0	99.886	0.456	0.969	0.999
	2.0	99.102	0.160	1.593	0.997
	3.0	98.776	0.033	2.207	0.993
0.5	0.5	99.954	0.511	1.093	0.999
	1.0	99.890	0.474	1.153	0.999
	2.0	99.491	0.222	1.706	0.998
	3.0	99.300	0.056	2.322	0.997
0.6	0.5	100.285	0.692	1.011	0.998
	1.0	100.227	0.653	1.057	0.999
	2.0	99.895	0.406	1.415	0.999
	3.0	99.603	0.114	2.199	0.997

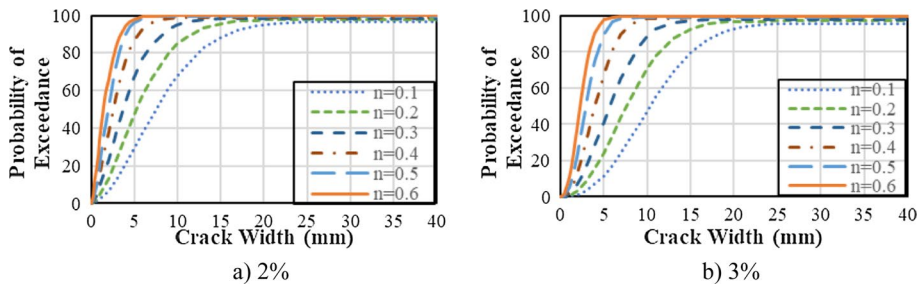


**Fig. 11** Probability curves of exceeding drift ratio value of (a) 2% and (b) 3% based on observed residual crack widths, for six different axial load ratios

crack width with a high axial load needs to be interpreted as substantial more displacement demands than for the lower axial load ratio.

## 6 Conclusion

A practical and efficient approach is proposed to estimate the maximum sustained drift demands based on post-earthquake residual flexural crack widths in reinforced concrete columns and beams. Simulation results are compared with the experimental results of column and beam tests with different properties such as axial load ratios, longitudinal reinforcement ratios, shear span ratios, etc. In addition, a one-bay one-story frame was tested by measuring crack widths at different displacement demands to investigate the accuracy of the model in predicting the cracking behavior of a RC structure. A parametric study is performed to investigate the residual crack width response of RC columns on dynamic loading conducted with the selected 11 earthquake motions. Forty-five thousand dynamic earthquake analyses are conducted, including different sectional properties and axial loads. Two equations are derived with regression analysis using all dynamic simulation results to estimate the maximum drift ratio obtained during the excitation. Finally, fragility responses of probability of exceedance of specific drift ratio with specific crack widths and maximum compressive strain values are provided. Following conclusions can be drawn:

- Although the determination of crack width in experiments is a challenging task, the maximum and residual crack width values in both RC members subjected to various deformation demands are estimated with sufficient accuracy using fiber-based frame elements with the section parameters calibrated by established methodology for both RC members.
- The maximum crack width value can be estimated from the total crack width results obtained from the simulation by calculating the number of cracks at the plastic hinge region, which is validated to be a reasonable assumption with the test results.
- Maximum and residual crack width estimations from the proposed model closely matched the measured crack widths and deformation responses for the new experimental test conducted on one-bay one-story RC frame for the purpose of this study to provide validation for the accuracy of the crack width estimations, affirming the reliability and applicability of the proposed methodology.

- The model calibrated with the provided methodology in this study has also the capability to represent the load–displacement response of the RC members and structure with good agreement.
- While the use of two extreme tensile plastic strain values in concrete material changes slightly in the load–displacement response estimation from the simulation of experimental studies, a significant effect on maximum and residual crack width estimation is obtained for some specimens. The sensitivity analysis shows that the robust nature of the approach and its ability of crack width predictions without significant dependence on the uncertainty of the input parameters,  $k_c$ ,  $k$ ,  $a$ ,  $a_1$ ,  $a_2$  and  $p_x$ . It was found that the expected uncertainty in the input parameters affected the crack width estimations by no more than about 7%.
- Strong correlation between the maximum drift ratio and total residual crack width and maximum compressive strain is obtained from parametric study with CC value of mostly higher than 0.8 for each different column sections including various longitudinal and transverse reinforcement ratios and axial loads.
- Notably, findings highlight the significant influence of axial load ratio on crack widths as well as maximum compressive strain. Higher axial loads correlate with smaller residual crack widths, with around 20% reduction observed for every 0.1 increase in axial load ratio. On the other hand, axial load ratio effect is reverse for maximum compressive strain. Substantial correlation can still be achieved with data which all different reinforcement ratios for the same axial load ratio are considered, as evidence by the correlation coefficients ranging from 0.80 to 0.94 for total residual crack width and maximum compressive strain, respectively.
- Two equations enabling the estimation of maximum drift ratios during the excitation based on either total residual crack width or maximum compressive strain at the plastic hinge region, considering the axial load ratio exhibit a high level of accuracy, with a mean absolute error of less than 0.06 for drift ratio estimation and strong correlation with the results from dynamic analysis with CC values of higher than 0.92 and lower RMSE values. Histograms of results from these two equations and dynamic analysis indicate their close relation.
- The proposed equation accurately predicts maximum drift ratios under dynamic displacement history from residual crack widths for Marder et al. (2018) column tests. For specimens with two different axial load ratios, the observed maximum drift ratio of 2.17% closely matched the equation's estimates of 2.36% and 2.09%, respectively, based on given parameters.
- The investigation into the probability of exceedance provides valuable insights into the relationship between crack width and the likelihood of surpassing specific drift ratio thresholds. Quantitative metrics, including cumulative distribution functions, provide precise estimations of the probability of structural performance exceeding critical thresholds. According to the results of this study, when the total residual crack width in the plastic hinge region exceeds approximately 3 mm, a RC column has exposed 2% drift ratios during EQ excitation with higher than %50 probability at higher axial load ratio levels (0.4 to 0.6). The conclusion is the same for 3% drift ratio with the higher axial load ratio range of 0.5 to 0.6. Conversely, for lower axial load ratios, the probability to exceed 2% and 3% drift ratios is significantly lower. While the lowest chance to pass %2 drift ratio with 5 mm residual crack width is around 30% for the axial load ratio of 0.1, the presence of such extensive cracking poses significant risk with 90% probability for columns the axial load ratio higher than 0.4.

In conclusion, this study contributes valuable insights into crack width estimation in RC members with a comprehensive investigation. The proposed approach demonstrates its accuracy and reliability by comparing simulation results with experimental data from various test configurations, including column and beam tests, as well as frame tests. The derived equations offer a practical, efficient and robust approach for estimating maximum drift demands based on post-earthquake residual crack widths. Measured residual crack widths after earthquake excitations on RC members can be used to determine the performance points of columns and beams for the structures. The outcomes provide engineers with practical tools for assessing structural performance and residual deformation capacity following seismic events. Additionally, the analysis of the probability of exceedance offers a quantitative framework for evaluating structural risk and remaining capacity, facilitating informed decision-making in demolition or strengthening efforts.

## 6.1 Recommendations

Several recommendations can be made to enhance further the understanding and practical application of the proposed approach in structural engineering practice in light of the findings and implications of this study. Firstly, conducting additional validation studies with more tests across a wider range of structural configurations, loading conditions, material properties and cross sections can be recommended with measuring residual crack widths and compressive strains. Thus, the robustness, effectiveness and applicability of the proposed methodology can be further verified and refined.

Furthermore, the sensitivity of residual crack width value to the several input parameters was investigated while it is important to note that the other parameters rather than  $\alpha_2$  used in the simulations were calibrated with the proposed methodology from the actual experimental results or suggested values from the literature and the focus was primarily on those parameters directly impacting the behavior of the materials and elements under consideration. Although numerous numerical simulations with various parameters were conducted within the focus of this study, additional validation problems with varying parameter values may provide further insights into the sensitivity of the results on these parameters.

As the primary focus of this study, flexural cracking is considered for the columns not expected to experience shear cracking. While there exist strong correlations between drift demands and flexural cracks based on the results in this study, combined flexural and shear cracking behavior triggers with different mechanisms and consequent failure modes than flexural only response. Therefore, although compressive failure, stirrup rupture and rebar buckling are implicitly considered in this study, further research may explore the interaction of all different cracking and failure types.

Lastly, the data generated with the provided model in this study can provide an opportunity to explore the integration of advanced technologies, such as machine learning and artificial intelligence, to further enhance the efficiency and accuracy of structural performance assessment. With this way, the process of crack width estimation and structural performance assessment can be automated efficiently.

**Author contributions** All authors contributed to the study conception and design. Data collection and numerical analysis were performed by Beyazit Bestami Aydin. Experiments were conducted by Beyazit Bestami Aydin and Saima Selin Aktas. The first draft of the manuscript was written by Beyazit Bestami



Aydin and all authors commented on previous versions of the manuscript. All authors read and approved the final manuscript.

**Funding** The authors declare that no funds, grants, or other support were received during the preparation of this manuscript.

**Data availability** The datasets generated during and/or analysed during the current study are available from the corresponding author on reasonable request.

## Declarations

**Conflict of interest** The authors have no relevant financial or non-financial interests to disclose.

**Open Access** This article is licensed under a Creative Commons Attribution 4.0 International License, which permits use, sharing, adaptation, distribution and reproduction in any medium or format, as long as you give appropriate credit to the original author(s) and the source, provide a link to the Creative Commons licence, and indicate if changes were made. The images or other third party material in this article are included in the article's Creative Commons licence, unless indicated otherwise in a credit line to the material. If material is not included in the article's Creative Commons licence and your intended use is not permitted by statutory regulation or exceeds the permitted use, you will need to obtain permission directly from the copyright holder. To view a copy of this licence, visit <http://creativecommons.org/licenses/by/4.0/>.

## References

- American Concrete Institute, ACI (2008) Guide for conducting a visual inspection of concrete in service. ACI Committee 201, Farmington Hills, Mich, USA
- American Society of Civil Engineers ASCE Standard ASCE, SEI, 41–17 (2017) Seismic evaluation and retrofit of existing buildings. American Society of Civil Engineers, Reston, Virginia, USA
- Japan building disaster prevention association (JBDPA) (1991) Guideline for post-earthquake damage evaluation and rehabilitation (in Japanese) (revised in 2001).
- Belarbi A, Hsu TTC (1994) Constitutive laws of concrete in tension and reinforcing bars stiffened by concrete. *ACI Struct J* 91(4):465–474
- Borosnyói A, Balázs GL (2005) Models for flexural cracking in concrete. The state of the Art. *Struct Concr* 6:53–62
- California Department of Transportation, AASHTO (2017) Caltrans bridge element inspection manual. Sacramento, California, USA.
- Castel A, Vidal T, François R (2012) Finite-element modeling to calculate the overall stiffness of cracked reinforced concrete beams. *J Struct Eng* 138(7):889–898. [https://doi.org/10.1061/\(ASCE\)ST.1943-541X.0000520](https://doi.org/10.1061/(ASCE)ST.1943-541X.0000520)
- Chen CC, Suswanto B, Lin YJ (2009) Behavior and strength of steel reinforced concrete beam–column joints with single-side force inputs. *J Constr Steel Res* 65(8–9):1569–1581. <https://doi.org/10.1016/j.jcsr.2009.04.003>
- Chiu CK, Sung HF, Chi KN, Hsiao FP (2019) Experimental quantification on the residual seismic capacity of damaged RC column members. *Int J Concr Struct Mater* 13:17
- EN 1992–1–1. Eurocode 2 (2004). Design of concrete structures.
- Faggella M, Barbosa AR, Conte JP, Spacone E, Restrepo JI (2013) Probabilistic seismic response analysis of a 3-D reinforced concrete building. *Struct Saf* 44:11–27. <https://doi.org/10.1016/j.strusafe.2013.04.002>
- Farhidzadeh A, Dehghan-Niri E, Moustafa A, Salamone S, Whittaker A (2013) Damage assessment of reinforced concrete structures using fractal analysis of residual crack patterns. *Exp Mech* 53:1607–1619. <https://doi.org/10.1007/s11340-013-9769-7>
- FEMA 306 (1997) Evaluation of earthquake damaged concrete and masonry wall buildings. Federal emergency management agency, Washington, D.C., United States.
- FEMA 307 (1998) Evaluation of earthquake damaged concrete and masonry wall buildings. Federal emergency management agency, Washington, D.C., United States.
- Hamidia M, Ganjizadeh A (2022) Computer vision-based automated stiffness loss estimation for seismically damaged non-ductile reinforced concrete moment frames. *Bull Earthq Eng* 20(12):6635–6658. <https://doi.org/10.1007/s10518-022-01408-w>
- Hu X, Chodora E, Prabhu S, Atamturktur S (2019) Extended constitutive relation error-based approach: the role of mass in damage detection. *Struct Control Heal Monit* 26:e2318. <https://doi.org/10.1002/stc.2318>

- Jamshidian S, Hamidia M (2023) Post-earthquake damage assessment for RC columns using crack image complexity measures. *Bull Earthq Eng* 21(13):6029–6063. <https://doi.org/10.1007/s10518-023-01745-4>
- Japan building disaster prevention association (JBDPA) (2014). Guideline for post-earthquake damage evaluation and rehabilitation (in Japanese).
- Kwak HG, Kim SP (2002) Cyclic moment–curvature relation of a RC beam. *Mag Concr Res* 54(6):435–447. <https://doi.org/10.1680/macrc.2002.54.6.435>
- Luo J, Liu G, Huang Z (2017) Damage detection for shear structures based on wavelet spectral transmissibility matrices under nonstationary stochastic excitation. *Struct Control Heal Monit* 24(1):e1862. <https://doi.org/10.1002/stc.1862>
- Madani HM, Dolatshahi KM (2020) Strength and stiffness estimation of damaged reinforced concrete shear walls using crack patterns. *Struct Control Heal Monit* 27:e2494. <https://doi.org/10.1002/stc.2494>
- Maeda M, Nakano Y, Lee KS (2004) Post-earthquake damage evaluation for R/C buildings based on residual seismic capacity. In: Proceedings of the 13th World Conference on Earthquake Engineering, August, Vol. 1179.
- Mander JB, Priestley MJN, Park R (1988) Theoretical stress-strain model for confined concrete. *J Struct Eng* 114(8):1804–1826. [https://doi.org/10.1061/\(ASCE\)0733-9445\(1988\)114:8\(1804\)](https://doi.org/10.1061/(ASCE)0733-9445(1988)114:8(1804))
- Marder K, Elwood KJ, Motter CJ, Clifton GC (2020) Post-earthquake assessment of moderately damaged reinforced concrete plastic hinges. *Earthq Spectra* 36(1):299–321. <https://doi.org/10.1177/8755293019878192>
- Marder K (2018) Post-earthquake residual capacity of reinforced concrete plastic hinges. PhD Dissertation, the University of Auckland, Auckland, New Zealand.
- Mazzoni S, McKenna F, Scott MH, Fenves GL (2006) OpenSees command language manual. *Pac Earthq Eng Res (PEER) Cent* 264(1):137–158
- McKenna F, Fenves GL (2000) An object-oriented software design for parallel structural analysis. Structures congress 2000. Advanced Technology in Structural Engineering.
- Nagarajaiah S, Yang Y (2017) Modeling and harnessing sparse and low-rank data structure: a new paradigm for structural dynamics, identification, damage detection, and health monitoring. *Struct Control Heal Monit* 24(1):e1851. <https://doi.org/10.1002/stc.1851>
- Nakano Y, Choi H, Takahashi N (2007) Residual seismic capacity estimation of RC frames with concrete block infill based on their crack widths. In: International Symposium on Seismic Risk Reduction, the JICA Technical Cooperation Project, Bucharest, Romania. (ISSR 2007), Paper ID 85.
- Palermo D, Vecchio FJ (2003) Compression field modeling of reinforced concrete subjected to reversed loading: formulation. *ACI Struct J* 100(5):616–625
- Paulay T, Priestley MN (1992) Seismic design of reinforced concrete and masonry buildings. Wiley Inc, New York
- Popovics SA (1973) Numerical approach to the complete stress-strain curve of concrete. *Cem Concr Res* 3(5):583–599. [https://doi.org/10.1016/0008-8846\(73\)90096-3](https://doi.org/10.1016/0008-8846(73)90096-3)
- Scott MH, Fenves GL (2006) Plastic hinge integration methods for force-based beam–column elements. *J Struct Eng* 132(2):244–252. [https://doi.org/10.1061/\(ASCE\)0733-9445\(2006\)132:2\(244\)](https://doi.org/10.1061/(ASCE)0733-9445(2006)132:2(244))
- Shiradhonkar SR, Sinha R (2018) Maximum and residual flexural crack width estimation in reinforced concrete frame members under seismic excitation. *J Struct Eng* 144(8):04018121. [https://doi.org/10.1061/\(ASCE\)ST.1943-541X.0002116](https://doi.org/10.1061/(ASCE)ST.1943-541X.0002116)
- Spacone E, Filippou FC, Taucer FF (1996) Fibre beam-column model for non-linear analysis of R/C frames: part I. Formulation. *Earthquake Eng Struct Dyn* 25:711–725. [https://doi.org/10.1002/\(SICI\)1096-9845\(199607\)25:7%3c711::AID-EQE576%3e3.0.CO;2-9](https://doi.org/10.1002/(SICI)1096-9845(199607)25:7%3c711::AID-EQE576%3e3.0.CO;2-9)
- Takahashi N, Nakano Y, Ito Y (2012) A quantification model for crack propagation of R/C members under earthquake loading. In: Proceedings of the Fifteenth World Conference on Earthquake Engineering, Paper ID 1874.
- Tan R, Hendriks MAN, Geiker M, Kanstad T (2020) Analytical calculation model for predicting cracking behavior of reinforced concrete ties. *J Struct Eng* 146(2):04019206. [https://doi.org/10.1061/\(ASCE\)ST.1943-541X.0002510](https://doi.org/10.1061/(ASCE)ST.1943-541X.0002510)
- Tao D, Zhang D, Li H (2013) Structural seismic damage detection using fractal dimension of time-frequency feature. *Key Eng Mater* 558:554–560. <https://doi.org/10.4028/www.scientific.net/KEM.558.554>
- Taucer F, Spacone E, Filippou FC (1991) A fiber beam-column element for seismic response analysis of reinforced concrete structures, (Second ed), Report no. UCB/EERC-91/17, Earthquake Engineering research center, University of California, Berkeley, CA
- Visintin P, Oehlers DJ, Muhamad R, Wu C (2013) Partial-interaction short term serviceability deflection of RC beams. *Eng Struct* 56:993–1006. <https://doi.org/10.1016/j.engstruct.2013.06.021>
- Yang T, Zo DQ (2013) Numerical simulation of crack growth of reinforced concrete beam based on XFEM. *J Zhejiang Univ Eng Sci* 47:495–501

- Yin GS, Zhou XF (2013) Crack propagation simulation based on extended finite element method. *J Changan Univ* 33:68–72
- Yu J, Yu K, Shang X, Lu Z (2016) New extended finite element method for pinching effect in reinforced concrete columns. *ACI Struct J* 113:689–699. <https://doi.org/10.14359/51688747>
- Yu JT, Zhan KL, Li LZ, Yu KQ (2018) Using x fem to model the effect of different axial compression on the hysteretic behaviour of the flexure-dominant rc columns. *Struct Des Tall Spec Build* 27:e1465. <https://doi.org/10.1002/tal.1465>

**Publisher's Note** Springer Nature remains neutral with regard to jurisdictional claims in published maps and institutional affiliations.

## Authors and Affiliations

**Beyazit Bestami Aydin**<sup>1,2</sup>  · **Baris Binici**<sup>1</sup> · **Saime Selin Aktas**<sup>1</sup> · **Max A. N. Hendriks**<sup>2,3</sup> · **Kagan Tuncay**<sup>1</sup>

✉ Beyazit Bestami Aydin  
B.B.Aydin@tudelft.nl

Baris Binici  
binici@metu.edu.tr

Saime Selin Aktas  
selin.aktas@metu.edu.tr

Max A. N. Hendriks  
m.a.n.hendriks@tudelft.nl

Kagan Tuncay  
tuncay@metu.edu.tr

<sup>1</sup> Department of Civil Engineering, Middle East Technical University (METU), Ankara, Türkiye, Turkey

<sup>2</sup> Faculty of Civil Engineering and Geosciences, Delft University of Technology (TU Delft), Delft, The Netherlands

<sup>3</sup> Department of Structural Engineering, Norwegian University of Science and Technology (NTNU), Trondheim, Norway